Application of Hybrid Numerical Method on the Influence Analysis of Bearing Number for Elliptic Aero-lubricated Bearing System

Cheng-Chi Wang[1], Ming-Yi Tsai [2]
[1] Department of Mechanical Engineering, Far East University, Tainan
[2] Department of Mechanical Engineering, Chin-Yi University of Technology, Taichung
NSC Project：NSC100-2628-E-269-016-MY2

Abstract

This paper employs a novel hybrid numerical method combining the differential transformation method (DTM) and the finite difference method (FDM) to analyze influence of bearing number and the nonlinear dynamic behavior of a rigid rotor supported by an elliptic aero-lubricated bearing (EAB) system. The results obtained for the orbits of the rotor center are in good agreement with those obtained using the traditional FDM approach. Moreover, the hybrid method avoids the divergence problem suffered by the FDM scheme at low values of the bearing number and computational time-step. The results presented summarize the changes which take place in the dynamic behavior of the EAB system as the bearing number is increased over the ranges 2.0 ~ 5.0, and therefore provide a useful insight into the nonlinear dynamics of the bearing system.

Keywords：Hybrid numerical method, Differential transformation method, Elliptic aero-lubricated bearing system

1. Introduction

Aero-lubricated bearings have a number of advantages compared to their rolling-element or oil-lubricated counterparts, including low friction losses and zero risk of contamination through lubricant leakage [1]. As a result, they are widely applied in a diverse range of rotatory systems. In a high speed rotational mechanical system, to prevent the damage caused by nonlinear vibration of gas film bearings and increase the stability of the system, circular gas bearings can be changed to noncircular bearing like tilting pad, off-set, multi-lobed, and elliptic bearings [2]. Tilting pad bearings are more suitable and better used for support of flexible rotor systems to control the appearance of instability, but the cost of manufacturing is too large. In order to design an economic bearing system, adequate to rigid rotor systems, elliptic bearings can be applied to increase the stability of rotor behavior.

The literature contains many investigations into the nonlinear dynamic response of rotor-bearing systems. For example, In 1983, Chandra et al. investigated static and dynamic characteristics of four noncircular gas journal bearing configurations. In this work, a modified Reynolds equation was solved by the finite element method and a comparative stability of four noncircular gas journal bearing configurations was done [3]. Sykes et al. [4] reported experimental observations of sub-harmonic motion in squeeze film bearings and suggested that such motion was a possible precursor of chaotic motion. Zhao et al. investigated the sub-harmonic and quasi-periodic motions of an eccentric squeeze film damper-mounted rigid rotor system. The authors showed that for large values of the rotor unbalance and static misalignment, the sub-harmonic and quasi-periodic motions generated at speeds of more than twice the system critical speed bifurcated from an unstable harmonic solution[5]. Sundararajan et al. utilized a simple shooting scheme integrated with an arc-length continuation algorithm to analyze the dynamics of periodically-forced rotor systems. The results revealed the occurrence of periodic, quasi-periodic or chaotic motion at different values of the rotor speed[6].

In 2006, Rahmatabadi et al. [7-8] studied the static and dynamic characteristics of noncircular gas journal bearings by considering the effect of mount angles and preload. They proved that noncircular bearings have better dynamic characteristic than circular bearings. Also, by using suitable value of mount angles stability margin can be increased. Although previous works provide insight into the behavior of the system but the nonlinear dynamic behavior of the gas film in a noncircular gas journal bearing has not examined. Therefore, this paper presents study of nonlinear dynamic behavior of a rigid rotor supported by two elliptic gas journal bearings.

In 2009, Zhou et al.[9] analyzed the bifurcation behavior of ultrashort self-acting gas journal bearings for MENS. The bearing system is modeled as a rigid rotor supported by bearing forces as a result of gas viscosity and rotational speed. Wang et al.[10-11] analyzed the bifurcation behavior and nonlinear dynamics of flexible and rigid rotors supported by gas journal bearings and showed that the rotors exhibited a complex dynamic behavior comprising periodic, sub-harmonic, and quasi-periodic responses at different values of the rotor mass and bearing number,

respectively.

The present study analyzes the nonlinear dynamic response of a rigid rotor supported by two elliptic gas journal bearings. In analyzing the bearing system, the time-dependent motions of the rotor center are described using the Reynolds equation. The modified Reynolds equation is solved using a hybrid numerical method combining the differential transformation method (DTM) and the finite difference method (FDM)[12-13]. The validity of the hybrid method is confirmed by comparing the results obtained for the orbits of the rotor center with those obtained using the conventional FDM scheme. The proposed method is then applied to analyze the nonlinear dynamic response of the rotor for rotor masses in the ranges 0.5 ~ 16.0kg.

2. Mathematica Modeling

2.1 Governing Equations

In this paper the elliptic aero-lubricated bearing (EAB) system is analyzed and composed by two arcs, and the centers of these two arcs are posited on the different sides of bearing center with the same distance shown in Fig. 1. O_J and O_B are the center of rotor and bearing, respectively. O_1 and O_2 are the centers of arcs. Cr is the bearing clearance. E is defined as the distance between the bearing center and arc center. The ellipticity ratio is expressed as:

$$E_r = \left(\frac{E}{C_r}\right),\ 0 \le E_r \le 1 \tag{1}$$

In Fig. 1, R_1 and R_2 are the radii of arcs. e1 and e2 are the distances between rotor center and arc center, respectively. e_{r1} and e_{r2} are the ellipticity ratios of arcs and expressed as following:

$$e_{r1} = \frac{e_1}{C_r} = \left[{e_{rB}}^2 + {E_r}^2 - 2e_{rB}E_r\cos(180-\alpha_B)\right]^{1/2} \tag{2}$$

where $e_{rB} = e_B / C_r$, $e_B = \overline{O_B O_J}$

$$\alpha_1 = \sin^{-1}\left[\frac{e_{rB}\sin\alpha_B}{e_{r1}}\right] \tag{3}$$

$$e_{r2} = \frac{e_2}{C_r} = \left[{e_{rB}}^2 + {E_r}^2 - 2e_{rB}E_r\cos\alpha_B\right]^{1/2} \tag{4}$$

$$\alpha_2 = \sin^{-1}\left[\frac{e_{rB}\sin\alpha_B}{e_{r2}}\right] \tag{5}$$

$$e_{rB} = n_B - E_r n_B \tag{6}$$

Where n_B=e/C_m, C_m: difference of bearing radius and rotor radius.

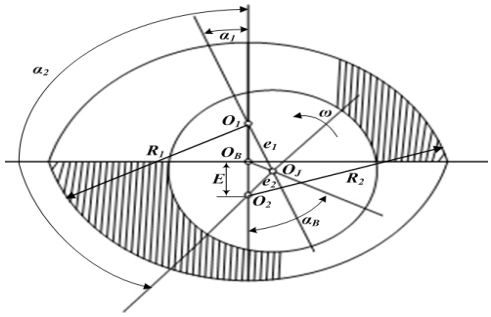

Fig. 1 Elliptic gas bearing system

In general, the pressure distribution in the gas film between the shaft and the bushing in an elliptic gas bearing system (EAB) is modeled using the compressible Reynolds' equation. In the present study, the time-dependent motions of the rotor center are modeled using the following modified non-dimensional Reynolds equation:

$$\frac{\partial}{\partial\phi}\left(H^3P\frac{\partial P}{\partial\phi}\right)+\frac{\partial}{\partial\theta}\left(H^3P\frac{\partial P}{\partial\theta}\right)=\Lambda\frac{\partial}{\partial\theta}(HP)+2\Lambda\frac{\partial}{\partial\tau}(HP) \tag{7}$$

where P is the dimensionless pressure corresponding to the atmospheric pressure P_a; H is the dimensionless gap between the rotating shaft and the bushing, corresponding to the radial clearance Cr; Λ is the bearing number; θand ϕ are the coordinates in the circumferential and axial directions, respectively.

The analysis presented in this study considers an EAB comprising a perfectly-balanced rigid rotor of dimensionless mass supported symmetrically on two identical elliptic aero-lubricated bearings, mounted in turn on rigid pedestals. Since the rotor is perfectly balanced and the EAB is symmetric about its central axes, the current analyses are confined to a single bearing supporting a rotating rotor of mass M_r with two degrees of translatory oscillation in the transverse plane.

In the transient state, the equation of motion of the rotor can be written as

$$M_r\frac{d^2X}{d\tau^2} = F_{elx} - F_{gfx} \quad , \quad M_r\frac{d^2Y}{d\tau^2} = F_{ely} - F_{gfy} \tag{8}$$

where F_{elx} and F_{ely} are the dimensionless external force in the x and y direction.

2.2 Numerical Simulations

In solving the modified Reynolds' equation using the finite difference method, Eq. (7) is discretized initially using the central-difference scheme in theθand ϕ directions and is then discretized once again using the implicit-back-difference scheme in the time domain τ. Note that for simplicity, a uniform mesh size is used. Eq (7) can be transformed into the following form:

$$3\left(H_{i,j}^{n+1}\right)^2\left(\frac{H_{i+1,j}^{n+1}-H_{i-1,j}^{n+1}}{2\Delta\theta}\right)\cdot\left(\frac{S_{i+1,j}^{n+1}-S_{i-1,j}^{n+1}}{2\Delta\theta}\right)+\left(H_{i,j}^{n+1}\right)^3\left(\frac{S_{i+1,j}^{n+1}-2S_{i,j}^{n+1}+S_{i-1,j}^{n+1}}{(\Delta\theta)^2}\right)+$$
$$3\left(H_{i,j}^{n+1}\right)^2\left(\frac{H_{i,j+1}^{n+1}-H_{i,j-1}^{n+1}}{2\Delta\phi}\right)\cdot\left(\frac{S_{i,j+1}^{n+1}-S_{i,j-1}^{n+1}}{2\Delta\phi}\right)+\left(H_{i,j}^{n+1}\right)^3\left(\frac{S_{i,j+1}^{n+1}-2S_{i,j}^{n+1}+S_{i,j-1}^{n+1}}{(\Delta\theta)^2}\right)$$
$$=2\Lambda\cdot H_{i,j}^{n+1}\left(\frac{P_{i+1,j}^{n+1}-P_{i-1,j}^{n+1}}{2\Delta\theta}\right)+2\Lambda P_{i,j}^{n+1}\left(\frac{H_{i+1,j}^{n+1}-H_{i-1,j}^{n+1}}{2\Delta\theta}\right)+$$
$$4\Lambda\cdot H_{i,j}^{n+1}\left(\frac{P_{i,j}^{n+1}-P_{i,j}^{n}}{\Delta\tau}\right)+4\Lambda\cdot P_{i,j}^{n+1}\left(\frac{H_{i,j}^{n+1}-H_{i,j}^{n}}{\Delta\tau}\right) \tag{9}$$

Gas pressure distribution at each time step can then be obtained using an iterative calculation process.

The hybrid numerical method proposed in this study is commenced by using the differential transformation method (DTM) to discretize the Reynolds' equation given in Eq. (7) with respect to time. DTM is one of the most widely used techniques for solving both linear and nonlinear differential equations due to its rapid convergence rate and minimal calculation error.[12-13]

In solving the Reynolds equation for the current EAB, DTM is used to transform the modified Reynolds' equation with respect to the time domain τ, and thus Eq. (7) becomes

$$3I\otimes\frac{\partial H}{\partial\theta}\otimes\frac{\partial S}{\partial\theta}+J\otimes\frac{\partial^2 S}{\partial\theta^2}+3I\otimes\frac{\partial H}{\partial\phi}\otimes\frac{\partial S}{\partial\phi}+J\otimes\frac{\partial^2 S}{\partial\phi^2} \tag{10}$$
$$=2\Lambda H\otimes\frac{\partial P}{\partial\theta}+2\Lambda P\otimes\frac{\partial H}{\partial\theta}+4\Lambda H\otimes\frac{\partial P}{\partial\tau}+4\Lambda P\otimes\frac{\partial H}{\partial\tau}$$

where

$$S(k)=P^2=P\otimes P=\sum_{l=0}^{k}P_{i,j}(k-l)P_{i,j}(l) \tag{11}$$

$$I(k)=H^2=H\otimes H=\sum_{l=0}^{k}H_{i,j}(k-l)H_{i,j}(l) \tag{12}$$

$$J(k)=H^3=H\otimes H\otimes H=\sum_{l=0}^{k}H_{i,j}(k-l)\sum_{m=0}^{l}H_{i,j}(l-m)H_{i,j}(m) \tag{13}$$

The finite difference method (FDM) is then used to discretize Eq. (10) with respect to the θ and ϕ directions. Note that Eq. (10) is discretized using the second-order-accurate central-difference scheme for both the first and the second derivatives.

Substituting Eqs. (11-13) into Eq. (10) yields

$$3\sum_{l=0}^{k}I_{i,j}(k-l)\sum_{m=0}^{l}\left(\frac{H_{i+1,j}(l-m)-H_{i-1,j}(l-m)}{2\Delta\theta}\right)\cdot\left(\frac{S_{i+1,j}(m)-S_{i-1,j}(m)}{2\Delta\theta}\right)$$
$$+\sum_{l=0}^{k}J_{i,j}(k-l)\left(\frac{Q_{i+1,j}(l)-2Q_{i,j}(l)+Q_{i-1,j}(l)}{(\Delta\theta)^2}\right)$$
$$3\sum_{l=0}^{k}I_{i,j}(k-l)\sum_{m=0}^{l}\left(\frac{H_{i,j+1}(l-m)-H_{i,j-1}(l-m)}{2\Delta\phi}\right)\cdot\left(\frac{S_{i,j+1}(m)-P_{i,j-1}(m)}{2\Delta\phi}\right) \tag{14}$$
$$+\sum_{l=0}^{k}J_{i,j}(k-l)\left(\frac{Q_{i,j+1}(l)-2Q_{i,j}(l)+Q_{i,j-1}(l)}{(\Delta\phi)^2}\right)$$
$$=2\Lambda\cdot\left[\sum_{l=0}^{k}H_{i,j}(k-l)\left(\frac{P_{i+1,j}(l)-P_{i-1,j}(l)}{2\Delta\theta}\right)\cdot\right]+2\Lambda\left[\sum_{l=0}^{k}P_{i,j}(k-l)\left(\frac{H_{i+1,j}(l)-H_{i-1,j}(l)}{2\Delta\theta}\right)\cdot\right]$$
$$+4\Lambda\left[\sum_{l=0}^{k}\left(\frac{l+1}{\tilde{H}}\right)P_{i,j}(k-l)\cdot H_{i,j}(l+1)\right]+4\Lambda\left[\sum_{l=0}^{k}\left(\frac{l+1}{\tilde{H}}\right)H_{i,j}(k-l)\cdot P_{i,j}(l+1)\right]$$

From Eq. (14), $P_{i,j}(k)$ is obtained for each time interval, where i and j are the coordinates of the node position and k indicates the *kth* term.

The motions of the rotor center are computed using an iterative procedure which commences by determining the acceleration and then computes the velocity and the displacement, on a step-by-step basis over time. In defining the initial conditions, the initial displacement is specified as the static equilibrium position of the shaft and defines the gap $H_{i,j}(k)$ between the shaft and the journal bearing, and the velocity of the rotor is assumed to be zero.

3. Results and discussion

In the second series of analyses, the rotor mass was specified as M_r =2.8kg and the bearing number Λ was increased over the range $2.0 \le \Lambda \le 5.0$.

3.1 Numerical Analysis

Table 1 compares the results obtained from the FDM and DTM&FDM for the orbits of the rotor center. It is observed that a good agreement exists between the two sets of results; particularly at higher values of the bearing number. Moreover, it can be seen that while the FDM method suffers numerical divergence at low values of the bearing number and time step, the DTM&FDM method converges under all the considered conditions and therefore represents a more appropriate method for analyzing the nonlinear dynamic response of the EAB.

Table 2 compares the Poincaré map data calculated by the DTM&FDM method using different time step values, $\tilde{H}$, for bearing number value. For a given rotor mass, the rotor center orbits are in agreement to approximately 4 decimal places for the different time steps, $\tilde{H}$.

Table 1 Comparison of rotor center orbits calculated by FDM and DTM&FDM methods, respectively.

Conditions		X(nT)	
		$\tilde{H}=0.001$	$\tilde{H}=0.01$
FDM	Λ=2.12	Divergence	0.1569118171
DTM&FDM		0.1561742179	0.1561540534
FDM	Λ=2.96	0. 8957028646	0. 8967048054
DTM&FDM		0.8952828731	0. 8952091462

Table 2 Comparison of Poincaré maps of rotor center with different values of Λ and $\tilde{H}$.

Λ= 2.12		
$\tilde{H}$	X (nT)	Y (nT)
π/300	0.1561747211	0.1871557321
π/600	0.156151034	0.1871862187
π/1200	0.1561815131	0.1871618113

3.2 Dynamic orbits

Fig. 2(a)-2(f) show that the dynamic orbits of the rotor center are regular at a low value of the bearing number (Λ=2.02), but become irregular at Λ=2.19. At a bearing number of Λ=2.44, the rotor center resorts to a regular periodic motion. When the bearing number is increased from 3.73 to 3.78, the orbits still exhibit a periodic characteristic. However, for higher bearing numbers of Λ=4.36, the rotor center performs a irregular motion.

3.3 Power spectra

Fig. 3(a)-3(f) show that the rotor center performs a sub-harmonic motion with a period of 2T at a bearing number of Λ=2.02. However, when the bearing number is increased to Λ=2.19, the power spectra (Fig. 3(b)) shows that the rotor center performs quasi-periodic motion. For values of Λ equal to 2.44, 3.73, and 3.78, the orbits have a sub-harmonic characteristic with a period of T, 2T, and 4T, respectively. Finally, for Λ=4.36, the rotor center performs quasi-periodic motion.

3.4 Bifurcation diagrams

Fig. 4 plots the bifurcation diagrams for the rotor center displacement in the horizontal and vertical directions as a function of the bearing number Λ in the range 2.0 to 5.0. In Fig. 4, it can be seen that the rotor center performs 2T-periodic motion over the bearing number range 2≤Λ<2.1. The 2T-periodic motion becomes unstable at bearing numbers of Λ=2.11 and is replaced by quasi-periodic motion. For bearing numbers in the range $2.11 \leq \Lambda \leq 2.72$(see Fig. 5(a)), the rotor center transits through Quasi→T→Quasi→T→Quasi→T motion. Then, the behavior of rotor center reverts to 2T- and 4T-periodic (sub-harmonic) motion for rotor mass values in the range 3.73≤Λ<3.78 and 3.78≤Λ<3.85, respectively. (see Fig. 5(b) and 5(c)) While for values of Λ in the interval $3.85 \leq \Lambda \leq 5$, the rotor transits through 2T→Quasi→2T→Quasi motion. In other words, these bearing number intervals, which correspond to the typical operating conditions of a real-world EAB, are characterized by T- and quasi-periodic motions of the rotor center. However, at higher bearing numbers, the rotor performs predominantly 2T-sub-harmonic and quasi-periodic motions in the horizontal and vertical directions. For example, Fig. 5(d) shows that at a bearing number of Λ=4.36, the rotor center performs quasi-periodic motion. Table 3 summarizes the motions performed by the rotor center for bearing number values in the interval $2.0 \leq \Lambda \leq 5.0$.

Table 3 Behavior of rotor center at different bearing numbers in interval $2.0 \leq \Lambda \leq 5.0$.

Λ	[2.0,2.11)	[2.11,2.12)	[2.12,2.19)
Dynamic Behavior	2T	**Quasi**	T
Λ	[2.19,2.44)	[2.44,2.93)	[2.93,2.96)
Dynamic Behavior	**Quasi**	T	**Quasi**
Λ	[2.96,3.73)	[3.73,3.78)	[3.78,3.85)
Dynamic Behavior	T	2T	4T
Λ	[3.85,4.36)	[4.36,4.62)	[4.62,4.76)
Dynamic Behavior	2T	**Quasi**	2T
Λ	[4.76,5.0]		
Dynamic Behavior	**Quasi**		

4. Conclusions

This study has utilized a hybrid numerical scheme comprising the differential transformation method (DTM) and the finite difference method (FDM) to analyze the nonlinear dynamic behavior of an elliptic aero-lubricated bearing system. The system state trajectories, Poincaré maps, power spectra, and bifurcation diagrams have revealed the presence of a complex dynamic behavior comprising periodic, sub-harmonic, and quasi-periodic responses of the rotor center. Although, this hybrid method might be not the best candidate, but from Table 1 the results obtained by the FDM and DTM&FDM methods for the orbits of the rotor center prove that a good agreement exists between different sets of results; particularly at higher values of the rotor mass. Moreover, the DTM&FDM method converges under all the considered conditions and therefore represents a more appropriate method for analyzing the nonlinear dynamic response of the EAB. The results of this study provide an understanding of the nonlinear dynamic behavior of elliptic aero-lubricated bearing systems characterized by different bearing number. Specifically, the results have shown that at a bearing number of Λ=2.19, the Poincaré map has the form of a closed curve, indicating that the rotor center performs quasi-periodic motion. This motion appears in

five bearing number intervals. As shown in Table 3, the intermediate intervals are characterized by T-, 2T-, and 4T-periodic motions.

5. Acknowledgment

This work was supported in part by the National Science Council, Taiwan under the Grants NSC 100-2628-E-269-016-MY2.

6. References

1. C. C. Wang, C. Y. Lo and C. K. Chen, Nonlinear Dynamic Analysis of a Flexible Rotor Supported by Externally Pressurized Porous Gas Journal Bearings, J. Tribology-Trans. of the ASME, Vol.124, No. 3, pp.553-561, 2002.
2. C. C. Wang, and C. L. Kuo, Nonlinear Dynamic Analysis of a Relatively Short Spherical Gas Journal Bearing System, J. Mechanical Science and Technology, Vol.24, No. 8, pp.1565-1571, 2010.
3. M. Chandra, M. Malik, and R. Sinhasan, Comparative Study of Four Gas-lubricated Noncircular Journal Bearing Configuration, Tribology International. Vol. 16, pp. 103-108, 1983.
4. J. E. H. Sykes, and R. Holmes, The Effect of Bearing Misalignment on the Non-linear Vibration of Aero-engine Rotor-damper Assemblies, Proceeding Institution of Mechanical Engineers, Vol. 204, pp. 83-99, 1990.
5. J. Y. Zhao, I. W. Linnett, and L. J. Mclean, Subharmonic and Quasi-periodic Motion of an Eccentric Squeeze Film Damper-mounted Rigid Rotor," ASME J. Vibration and Acoustics, Vol. 116, pp. 357-363, 1994.
6. P. Sundararajan, and S. T. Noah, Dynamics of Forced Nonlinear Systems Using Shooting /arc-length Continuation Method Application to Rotor Systems, ASME J. Vibration and Acoustics, Vol. 119, pp. 9-20, 1997.
7. A. D Rahmatabadi, and R. Rashidi, Effect of Mount Angle on Static and Dynamic Characteristics of Gas-lubricated Noncircular Journal Bearings, Iranian Journal of Science and Technology Transaction B-Engineering. Vol. 37, pp. 27-37, 2006.
8. A. D Rahmatabadi, M. Nekoeimehr, and R. Rashidi, Micropolar Lubricant Effects on the Performance of Noncircular Lobed Bearings, Tribology International, Vol. 4, pp. 33-38, 2007.
9. J. B. Zhou, G. Meng, J. Y. Chen, and W. M. Zhang, Bifurcation Analysis of Ultrashort Self-acting Gas Journal Bearings for MEMS, IEEE Transactions on Industrial Electronics. Vol. 56, pp. 3188-3194, 2009.
10. C. C. Wang, Theoretical and Nonlinear Behavior Analysis of a Flexible Rotor Supported by a Relative Short Herringbone-grooved Gas Journal-bearing System, Physica D-Nonlinear Phenomena, Vol. 237, pp. 2282-2295, 2008.
11. C. C. Wang, Application of a Hybrid Method to the Nonlinear Dynamic Analysis of a Spherical Gas Journal Bearing System, Nonlinear Analysis -Theory, Methods & Applications, Vol. 70, pp. 2035-2053, 2009.
12. C. C. Wang, and H. T. Yau, Application of the Differential Transformation Method to Bifurcation and Chaotic Analysis of an AFM Probe Tip, Computers & Mathematics with Applications, Vol.61, No. 8, pp.1957-1962, 2011.
13. C. C. Wang, Application of a Hybrid Method to the Bifurcation Analysis of a Relative Short Gas Journal Bearing System with Herringbone Grooves, Industrial Lubrication and Tribology, Vol.63, No. 5, pp.307-319, 2011.

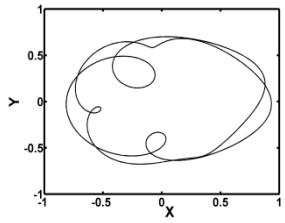

2(a)

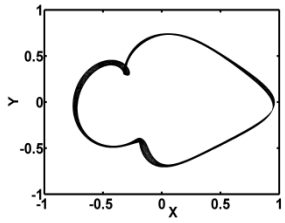

2(b)

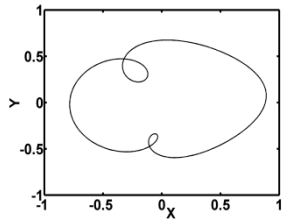

2 (c)

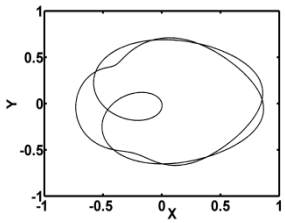

2(d)

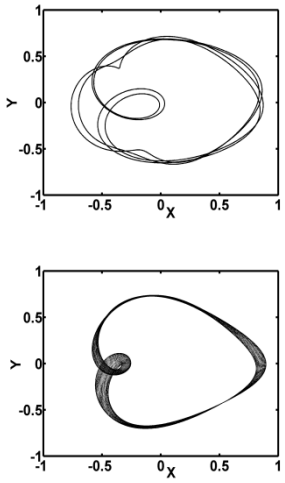

2(e) 2(f)

Fig. 2 Trajectories of rotor center at Λ= 2.02, 2.19, 2.44, 3.73, 3.78, 4.36 (Fig. 2(a)-2(f))

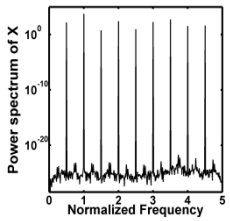

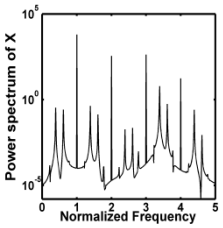

3(a) 3(b)

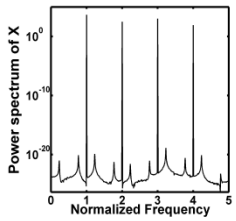

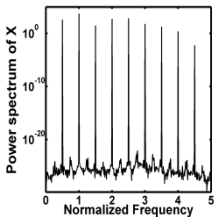

3(c) 3(d)

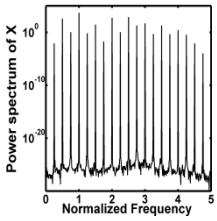

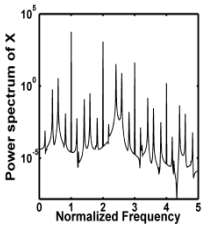

3(e) 3(f)

Fig. 3 Power spectra of rotor center in horizontal direction at Λ= 2.02, 2.19, 2.44, 3.73, 3.78, 4.36 (Fig. 3(a)-3(f))

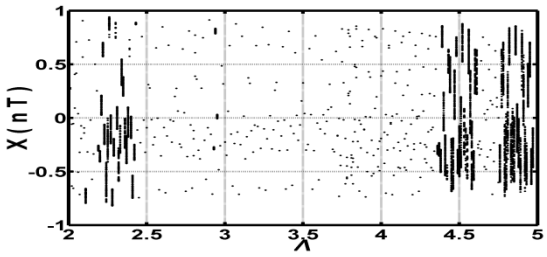

4(a)

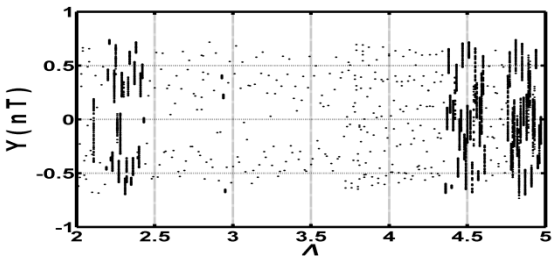

4(b)

Fig. 4 Bifurcation diagrams: (a)X(nT) and (b)Y(nT) versus bearing number over interval $2 \leqq \Lambda \leqq 5$.

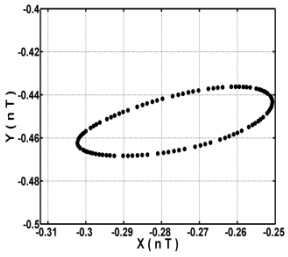

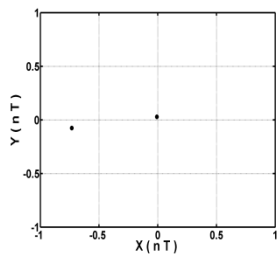

5(a) 5(b)

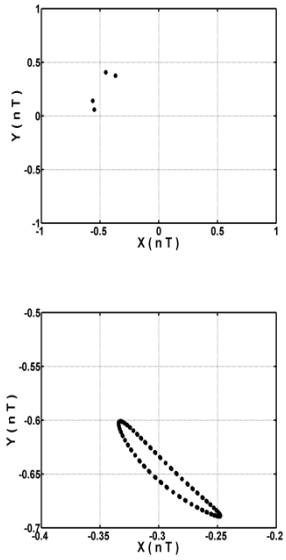

5(c) 5(d)

Fig. 5 Poincaré maps of rotor center trajectory at (a) Λ=2.19, (b) 3.73, (c) 3.78 (d) 4.36.

應用混合數值法分析軸承數對橢圓形氣潤軸承系統之影響

汪正祺[1]、蔡明義[2]
[1]遠東科技大學機械工程系
[2]勤益科技大學機械工程系

摘要

在本論文中，主要分析有關剛性轉子於橢圓形氣潤軸承系統之非線性動態行為。本文中提出一個與時間具有相關性的氣體軸承，並採用混合數值法來求解雷諾方程式(Reynolds equation)。此混合法主要結合微分換法及有限差分法，再利用系統的軌跡圖、龐卡萊映射(Poincare map)、頻率響應和分岔圖(Bifurcaton diagrams)來分析系統在不同的軸承數(bearing number)之下，轉子中心在水平及垂直方向的動態行為。研究顯示數值結果具有良好的收斂性，且轉子中心的動態行為相當複雜包含有週期和準週期運動(Quasi-periodic)現象，此結果可做為後續軸承系統設計之依據。

關鍵字:混合數值法、微分轉換法、橢圓形氣潤軸承